RSC Advances

PAPER

View Article Online
View Journal | View Issue

Cite this: *RSC Adv.*, 2017, **7**, 24046

The effect of acid treatment on the active sites and reaction intermediates of the low-cost TS-1 in propylene epoxidation†

Guang Xiong,* Qianying Jia, Yuanyuan Cao, Liping Liu and Zhendong Guo

This study investigated the roles of the different titanium species of low-cost TS-1 in propylene epoxidation and the influence of acid treatments. The low-cost TS-1 zeolites with different titanium species were synthesized using the hydrothermal method and characterized by ultraviolet (UV)-Raman, X-Ray Diffraction (XRD), ultraviolet visible diffuse reflectance spectroscopy (UV-Vis), N_2 physical absorption and NH_3 temperature programmed desorption (NH_3-TPD) techniques. The roles of the different titanium species in the low-cost TS-1 samples were investigated by gas chromatography-Raman spectrometry (GC-Raman) during the propylene epoxidation process. The framework titanium species was found to be active for propylene epoxidation, while the extra-framework Ti species were found to be harmful for propylene epoxidation due to their acidity. The extra-framework Ti species can be removed by acid treatments. It was found that the acid treatment of the as-synthesized TS-1 is more effective since the amorphous TiO_2 was not transformed into anatase TiO_2 upon calcination. Strong acids, such as HCl, HNO_3 and H_2SO_4, are more efficient for the elimination of the extra-framework TiO_2, but do not significantly affect the framework titanium species. After treatment with an acid of a suitable concentration, the amount of the active intermediate species Ti–OOH(η^2) can be increased, and a higher conversion of propylene and yield of PO can be achieved.

Received 13th March 2017
Accepted 17th April 2017

DOI: 10.1039/c7ra02983g

rsc.li/rsc-advances

1. Introduction

The system of titanium silicalite (TS-1) and H_2O_2 has been an important topic in green catalytic chemistry for decades because of its unique catalytic properties in oxidation reactions under mild conditions.[1–5] The classical method was used to produce TS-1 with the crystal size of 100–200 nm, which exhibited good catalytic properties. However, the template tetrapropyl ammonium hydroxide (TPAOH) used in the classical method is expensive, which restrains its applications in industry. Some attempts have been made to reduce the amount of the template TPAOH required. Deng[6] carried out hydrothermal synthesis of TS-1 with a lower ratio of TPAOH/SiO_2 in two-step and multistep hydrolysis processes by fine tuning the nucleation and growth step during crystallization, which showed good activity in the oxidation of alkene and ammoximation of ketone. To further reduce the cost of the catalyst, tetrapropyl ammonium bromide (TPABr) was used as a template for the synthesis of TS-1.[7] However, the catalytic performance of the low-cost TS-1 is not as good as that of the classical TS-1. Therefore, post-treatments have been used to further improve the catalytic properties of the low-cost TS-1. Li[8] reported the acid treatment of the low-cost TS-1, and the catalytic activity in the propylene oxidation reaction showed a large improvement because of the elimination of the non-framework titanium species. In addition, the alkali treatment is a common method in improving the catalytic performance of the TS-1 zeolite. Tsai[9] reported the alkali treatment of TS-1 using NaOH, leading to the generation of the mesopore and subsequently an increase in the catalytic activity. Tuel[10,11] put forward the dissolution–recrystallization method using the TPAOH to improve the diffusion of TS-1.

In addition, the roles of different titanium species in the classical TS-1 during the propylene epoxidation process have been studied.[12,13] It was accepted that the isolated titanium species in the framework of the TS-1 zeolite is the active site for the selective oxidation. The non-framework Ti species is harmful for the epoxidation reactions. It was found that the acidity of the amorphous Ti species is stronger than that of the anatase TiO_2, which leads to undesired side reaction.[13] For the low-cost TS-1 zeolite, the distribution of the titanium species is more complicated. Therefore, to improve its catalytic properties, a systematic study on the distribution and the roles of the different titanium species, before and after the post-treatment, are highly required to be known.

Raman spectroscopy has been proven to be a powerful tool to identify the different Ti species by changing the wavelength of

State Key Laboratory of Fine Chemicals, School of Chemical Engineering, Dalian University of Technology, Dalian 116024, China. E-mail: gxiong@dlut.edu.cn; Fax: +86-411-84986340

† Electronic supplementary information (ESI) available. See DOI: 10.1039/c7ra02983g

the excitation source, particularly under reaction conditions.[13–16] Three resonance enhanced Raman bands at 490, 530, and 1125 cm^{-1} obtained with the use of a 244 nm laser line are the typical peaks of the isolated tetrahedral titanium species in the framework of TS-1. In the spectra excited by the 325 and 532 nm lines, the bands at 144, 390, 515, and 637 cm^{-1} are ascribed to anatase TiO_2. The band at 700 cm^{-1} was assigned to the amorphous Ti species. Raman spectroscopy has also been used to investigate the reaction intermediates on the TS-1 for propylene epoxidation. The reaction intermediate Ti–OOH(η^2) is found to be crucial for propylene epoxidation, whose typical peak is located at 837 cm^{-1}.[16]

Our previous studies mainly focused on the classical TS-1 when the expensive TPAOH was used as a template. In this study, the low-cost TS-1 zeolite containing different titanium species was synthesized by changing the Ti/Si ratio and synthesis conditions. Then, the technique of gas chromatography-Raman spectroscopy (GC-Raman)[13] was used to study the relationship between the amount of active intermediate, the product propylene epoxide (PO) and the conversion of propylene. The roles of different titanium species in low-cost TS-1 for propylene epoxidation are discussed herein. Furthermore, the post treatment with different acids was used to eliminate the extra-framework Ti-species of the TS-1. The effects of the acid treatment on the Ti distribution, the reaction intermediates and the catalytic properties were investigated using the GC-Raman technique.

2. Experimental

2.1 Synthesis

2.1.1 Materials. Chemical reagents included colloidal silica (30 wt%, SiO_2) (CP, Qingdao Chengyu Chemical Co., Ltd.), titanium tetrachloride ($TiCl_4$) (AR, Damao Chemical Co., Ltd.), tetrapropylammonium hydroxide (TPAOH, 1.23 M solution in water) (Shanghai Cairui Chemical Co., Ltd.), tetrapropylammonium bromide (TPABr) (CP, Shanghai Cairui Chemical technology Co., Ltd.), isopropyl alcohol (IPA) (AR, Tianjin Fuyu Chemical Co., Ltd.), and ethylamine (65 wt%, EA) (AR, Tianjin Fuchen Chemical Co., Ltd.).

2.1.2 Synthetic procedure. $TiCl_4$ was hydrolyzed in IPA. The colloidal silica and deionized water were mixed. Hydrolyzed $TiCl_4$ was added dropwise to the colloidal silica solution. Then, the template TPABr, the base EA, the seed (nanosized, synthesized according to the literature[2]) and deionized water were added to the mixture. Finally, the gel was crystallized at 170 °C for 3 days in a 100 mL autoclave. The molar compositions of the final synthesis gels were as follows: 1.0SiO_2 : (0–0.3)TiO_2 : (0.1–0.3)TPABr : 30 H_2O : 1.0 IPA : 0.15 ethylamine. The solid product was filtered, washed with distilled water, dried at 100 °C overnight and calcined at 550 °C for 10 h to remove the template. TS-1 samples with different titanium distributions were synthesized by adjusting the SiO_2/TiO_2 ratios.

2.2 Acid treatment

The TS-1 sample with a SiO_2/TiO_2 molar ratio of 30 was treated for 24 h with an acid modifier at a liquid to solid ratio of 50 mL g^{-1}. Following this, the solution was centrifuged, washed with distilled water, dried at 100 °C overnight and calcined at 550 °C for 10 h.

2.3 Characterization

X-ray powder diffraction (XRD) patterns were recorded on a Rigaku D/MAX-2400 using Cu Kα radiation with a scanning rate of 4° min^{-1}.

Ultraviolet-visible diffuse reflectance spectra (UV-Vis) were obtained on a SHIMADZU UV-240 spectrometer using $BaSO_4$ as a reference.

Nitrogen physisorption measurements were performed on a Quantachrome Autosorb-1-MP adsorption porosimeter at 77 K. All samples were degassed at 623 K for 3 h under vacuum. The specific surface area and the micropore volume were calculated by the BET method and the *t*-plot method, respectively. The total pore volume was determined at a relative partial pressure P/P_0 of 0.99.

Scanning electron microscopy (SEM) was carried out on a Hitachi S-4800 instrument operating at 3 kV.

The NH_3-TPD was performed on a ChemBET 3000 chemisorb apparatus from Quantachrome. The rate of ammonia desorption was monitored continuously with a thermal conductivity detector (TCD).

Raman spectra were recorded on a DL-2 Raman spectrometer with a collection time of 300 s. A 244 nm line of LEXEL LASER and 325 nm line of a He–Cd laser were used as excitation sources. The laser power at the samples was less than 5 mW. An Acton triple monochromator was used as a spectrometer for Raman scattering. The spectra were collected using a Priston CCD detector. During the *in situ* experiments, the TS-1 sample (0.05 g) was moved into a stainless steel cell equipped with a quartz window after the addition of $H_2O_2/H_2O/CH_3OH$ solution. Propylene (3% propylene and 97% helium gas in volume fraction) was introduced into the cell at a flow rate of 25 mL min^{-1}. The spectra during the reaction process were recorded by the UV-Raman spectrometer. Moreover, the component analysis of the output gas was detected on a GC 9790 gas chromatograph, using a flame ionization detector and a capillary column (PEG-20M, 30 m). The concentration of propylene oxide (PO) was presented directly by its peak area in the GC spectra. The peak area was integrated by the OriginPro (8.0) program.

3. Results and discussion

3.1 Catalyst characterization

3.1.1 XRD. In this study, to understand the role of the framework and non-framework Ti species of the low-cost TS-1, the TS-1 with the SiO_2/TiO_2 ratios of 30 and 120 were synthesized. The TS-1 (SiO_2/TiO_2 ratio = 120) was expected to contain only framework Ti species, while the TS-1 (SiO_2/TiO_2 ratio = 30) should contain both framework and non-framework Ti species. Both the samples can be used to study the effect of non-framework Ti species of low-cost TS-1. Furthermore, the TS-1 samples with the SiO_2/TiO_2 ratios of 100, 110, and 120 were

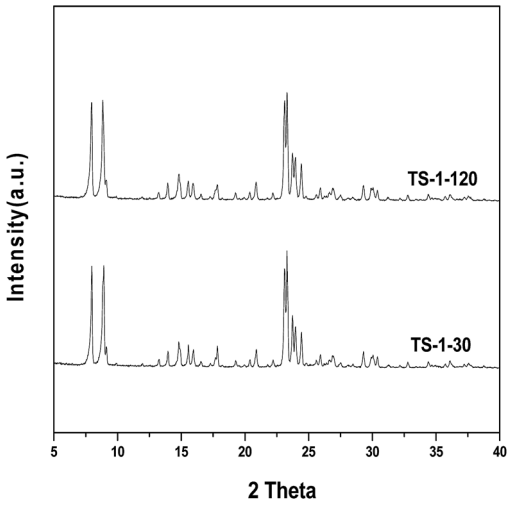

Fig. 1 XRD patterns of the TS-1 samples with different SiO_2/TiO_2 ratios.

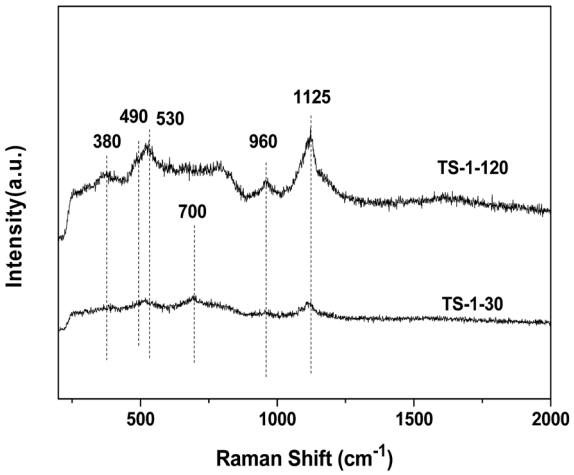

Fig. 3 UV-Raman spectra of the TS-1 samples with different SiO_2/TiO_2 ratios.

used to study the role of the framework titanium species, which will be discussed later in the ESI (see part A in the ESI†).

The XRD patterns of the TS-1 samples with different SiO_2/TiO_2 ratios are shown in Fig. 1. Both samples exhibit the characteristic peaks at $2\theta = 7.8°$, 8.8°, 23.2°, 23.8° and 24.3°, which are typical for MFI topology.

3.1.2 UV-Vis. UV-Vis spectra of the TS-1 samples with different SiO_2/TiO_2 ratios are shown in Fig. 2. The three adsorption peaks located at 210–220, 270 and 320 nm are assigned to the tetrahedrally coordinated framework Ti species,[17] amorphous Ti species[18] and anatase TiO_2, respectively. It is clear that the TS-1-30 sample consists of the framework Ti species, amorphous Ti species and anatase TiO_2, while the TS-1-120 sample contains only the framework Ti species. Moreover, the amount of framework titanium species in TS-1-30 is higher than that of the TS-1-120 sample.

3.1.3 Raman. Fig. 3 shows the Raman spectra of the TS-1 samples with different SiO_2/TiO_2 ratios collected with a 244 nm laser line. The peaks at 380, 490, 530, 700, 960 and 1125 cm^{-1} are observed in the spectra. The peak at 380 cm^{-1} is characteristic of MFI topology. The band at 960 cm^{-1} has been assigned to the Ti–O stretching, titanyl group Ti=O, silanol group Si–OH, titanium related defect sites or the Ti–O–Si bridge. The peaks at 490, 530 and 1125 cm^{-1} are characteristic of the framework Ti species. The TS-1-30 also shows a band at 700 cm^{-1}, which is assigned to the amorphous Ti species.[19] Compared with the spectra of TS-1-120, the intensities of all peaks for the sample TS-1-30 are distinctly weak, which is due to the strong absorption of UV light by the non-framework Ti species.

Fig. 4 shows the Raman spectra of the TS-1 samples with different SiO_2/TiO_2 ratios collected with a 325 nm laser line. The TS-1-30 sample shows the Raman bands at 144, 390, 518 and 635 cm^{-1}, which are typical for the anatase TiO_2. In comparison, the bands of anatase TiO_2 are absent in the spectrum of the TS-1-120 sample. The TS-1-120 sample shows the peaks at 380, 817, 960 and 1125 cm^{-1}, which are assigned to the MFI

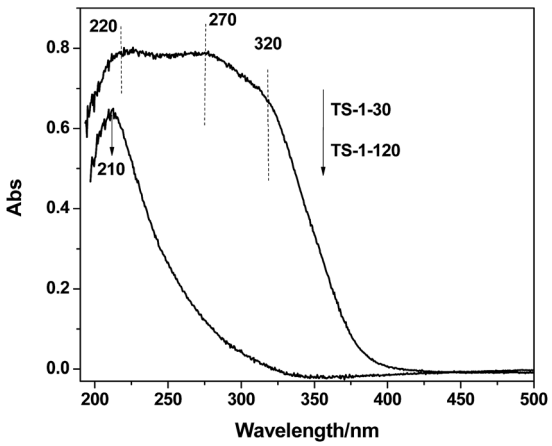

Fig. 2 UV-Vis spectra of the TS-1 samples with different SiO_2/TiO_2 ratios.

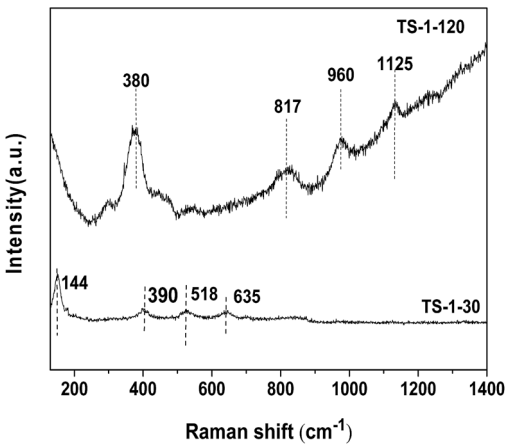

Fig. 4 Raman spectra of the TS-1 samples with different SiO_2/TiO_2 ratios (325 nm).

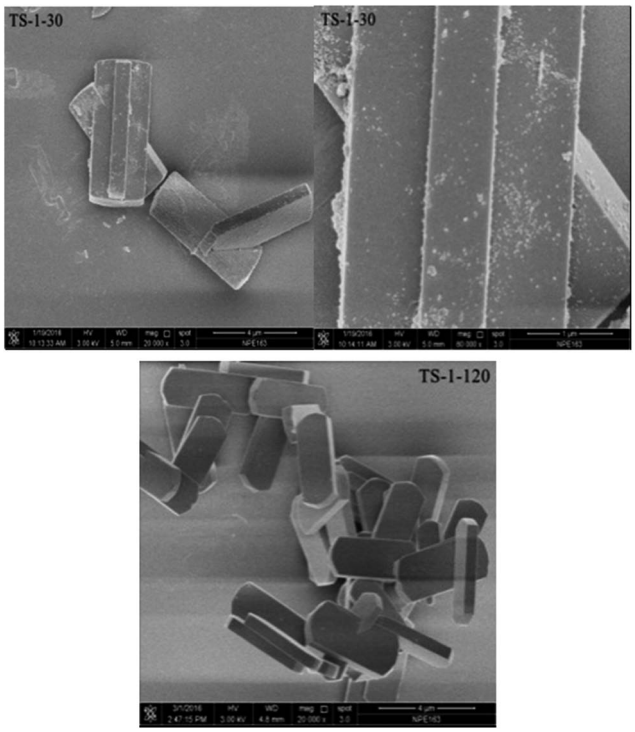

Fig. 5 SEM images of the TS-1 samples with different SiO_2/TiO_2 ratios.

structure. The Raman results further confirm that TS-1-120 contains only framework Ti species, while TS-1-30 contains the framework Ti species, amorphous TiO_2 and anatase TiO_2. This is consistent with the UV-Vis result (see Fig. 2).

3.1.4 SEM. Fig. 5 shows the SEM images of the low-cost TS-1 samples with the SiO_2/TiO_2 ratios of 30 and 120. The TS-1 samples show a coffin-like morphology with a crystal size of about 5 μm × 2.5 μm × 0.5 μm. The surface of the TS-1-30 sample is rough due to the presence of the non-framework TiO_2, while that of the TS-1-120 sample is smooth.

3.1.5 NH_3-TPD. Fig. 6 shows NH_3-TPD profiles of the TS-1 samples with different Ti species. The TS-1-120 sample shows

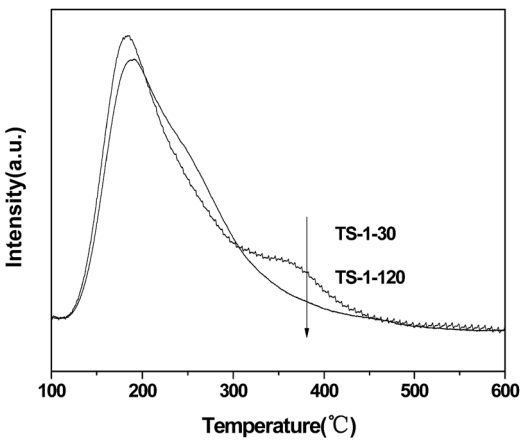

Fig. 6 NH_3-TPD profiles of the TS-1 samples with different SiO_2/TiO_2 ratios.

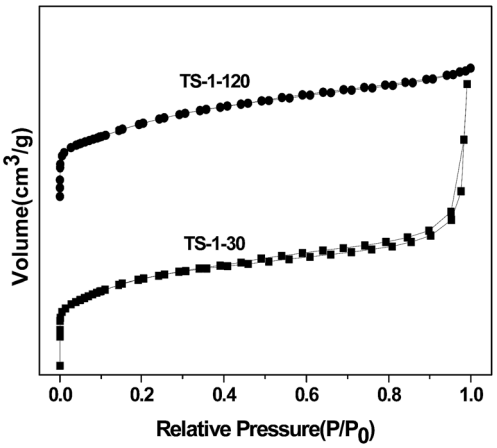

Fig. 7 N_2 adsorption isotherms of the TS-1 samples with different SiO_2/TiO_2 ratios.

a desorption peak at around 200 °C, indicating that only the weak acid site was observed on the TS-1 species, which contained the framework Ti species. In addition to the low-temperature desorption peak, the TS-1-30 sample also shows the desorption peak at higher temperatures, indicating the presence of strong acid sites. Considering that the titanium-rich samples (TS-1-30) contain non-framework Ti species, a close correlation exists between the non-framework Ti species and the strong acid sites.

3.1.6 N_2-Physical adsorption. Fig. 7 shows the N_2 adsorption isotherms of the TS-1 samples with different SiO_2/TiO_2 ratios. A sharp increase in nitrogen adsorption at $P/P_0 = 0.01$ indicates the presence of micropores. In addition, compared to the TS-1-120 sample, the TS-1-30 sample also presents an abrupt jump at high relative pressure. This is probably due to the formation of the macropores in between the crystal and TiO_2. The SEM image (see Fig. 5) shows that the surface of the TS-1-120 sample is very smooth. In contrast, the TS-1-30 sample is rough and has numerous small particles adhered onto the surface. This may cause the abrupt jump at high relative pressure.

Table 1 shows the textural properties of the TS-1 samples with different SiO_2/TiO_2 ratios. It can be seen that the BET surface area, the microporous surface area and the microporous volume of the TS-1-30 sample are all lower than that of the sample with high SiO_2/TiO_2 ratio (120). From the previous result, we know that the sample of SiO_2/TiO_2 ratio = 30 contains the non-framework Ti species, which may block the channels to some extent.

3.2 *In situ* GC-Raman results

3.2.1 The role of the non-framework Ti species of the low-cost TS-1. The role of the isolated Ti species in the framework of the low-cost TS-1 zeolite has been investigated in part A of the ESI.† The TS-1 with SiO_2/TiO_2 ratios of 100, 110 and 120, which contain only the framework Ti species, were used as the model catalysts. A positive correlation among the concentration of the framework Ti species, the amount of reaction intermediate Ti–

Table 1 Textural properties of the TS-1 samples with different SiO_2/TiO_2 ratios

Samples	S_{BET} ($m^2\ g^{-1}$)	S_{micro} ($m^2\ g^{-1}$)	S_{ext} ($m^2\ g^{-1}$)	V_{total} ($cm^3\ g^{-1}$)	V_{micro} ($cm^3\ g^{-1}$)	V_{meso} ($cm^3\ g^{-1}$)
TS-1-30	389.9	355.1	34.8	0.2382	0.1501	0.0881
TS-1-120	440.8	392.5	48.3	0.2379	0.1821	0.0558

OOH(η^2), the propylene conversion and the yield of the PO has been established. Our previous studies[13,16] indicated that an important active site of TS-1 is TiOOH(η^2), which is formed by the interaction between the framework Ti species and H_2O_2. The framework Ti species can expand the tetrahedral coordination through the interaction with H_2O_2 or a solvent to achieve the octahedral coordination. This result indicates that the isolated Ti species in the framework of the low-cost TS-1 zeolite is the active center for the propylene epoxidation. Subsequently, the TS-1 with SiO_2/TiO_2 ratios of 120 and 30 were investigated using the *in situ* Raman-GC technique. After dropping 30 μL of $H_2O_2/H_2O/CH_3OH$ solution (the volume ratio of H_2O_2 and CH_3OH in the solvent is 1 : 1) on the TS-1 sample (0.05 g), the Raman spectra of the TS-1/H_2O_2/H_2O/CH_3OH system, under a continuous flow of propylene, were collected. Methanol was added because it is the best solvent for liquid phase epoxidation of alkenes. The Raman spectra of the TS-1/H_2O_2–H_2O/CH_3OH system are shown in Fig. 8. It can be seen that the evolution of the Raman spectra of the abovementioned system with different Ti species distributions are similar. In the beginning of the reaction, the bands at 490, 530, and 1125 cm^{-1} are extremely quenched immediately. The band at 1125 cm^{-1} shifts to 1134 cm^{-1}, which has been attributed to the expansion of the Ti coordination sphere. Once the Ti coordination sphere expands, the Td-like symmetry of the Ti(IV) species is destroyed, and the symmetry of the vibrational modes is no longer the same as that of the LMCT. A new shoulder at 618 cm^{-1} is attributed to the symmetric breathing mode of the $Ti(O_2)^-$ cycle.[20]

Moreover, the feature at 837 cm^{-1}, which has been assigned to a Ti–OOH(η^2) species, appears quickly. The intensity of the band at 837 cm^{-1} first increases and then drops gradually as time passes. At the same time, the peak area of PO in the GC spectra shows the same trend, which indicates good correlation. A band at 1644 cm^{-1}, which is related to propylene physisorbed into the zeolite channels, appears and its intensity increases with increasing the reaction time.

Fig. 9 shows the variation trend of the characteristic peak as the reaction time increases. As shown in Fig. 9, the amount of the active intermediate Ti–OOH(η^2) on the TS-1-30 is lower than that on TS-1-120, although the concentration of the framework Ti

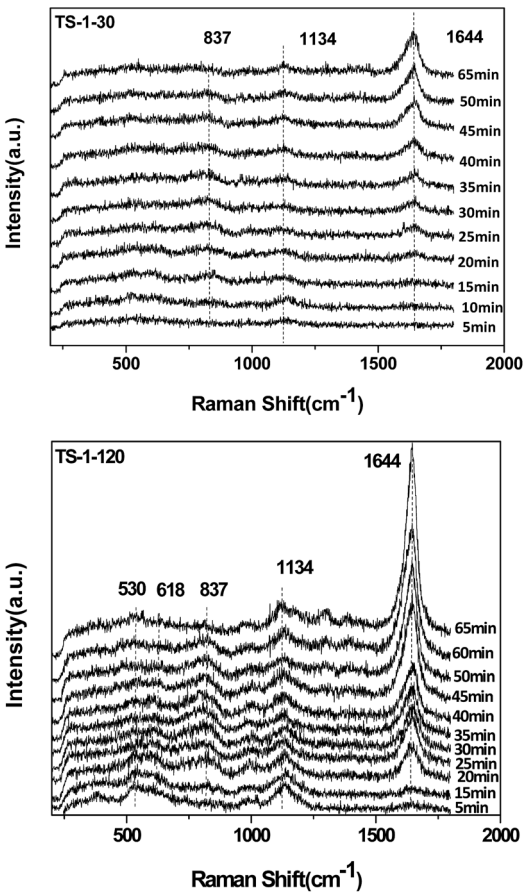

Fig. 8 *In situ* Raman spectra of the TS-1/H_2O_2–H_2O/CH_3OH system obtained at different times during the methanol-included epoxidation reaction, collected with a 244 nm laser line.

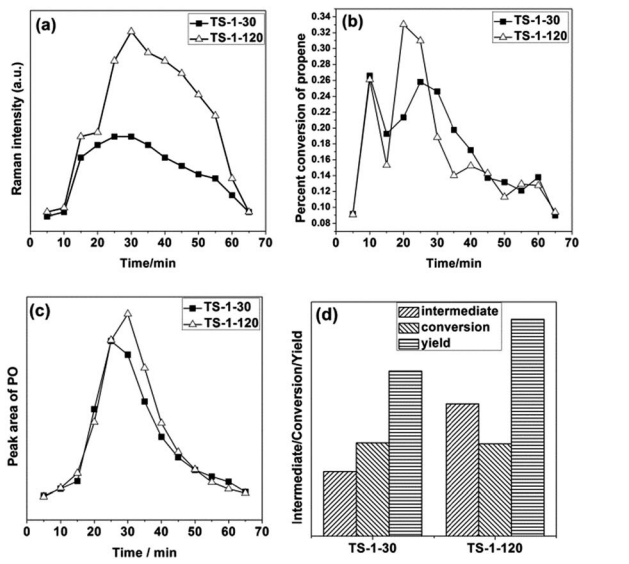

Fig. 9 (a) The UV-Raman intensity of the 837 cm^{-1} band at different times during the epoxidation reaction. (b) The percent conversion of propene in the TS-1/H_2O_2–H_2O/CH_3OH system at different times. (c) The peak area of PO in the GC spectra at different times. (d) The total column of the intermediate, conversion and yield with different SiO_2/TiO_2 ratios.

species of TS-1-30 is higher than that of TS-1-120 (see Fig. 2). The result indicates that the existence of the non-framework Ti species influences the formation of the active intermediate Ti–OOH(η^2). The H_2O_2 decomposition is not taken into account in this study due to the low reaction temperature. One possibility is that the non-framework Ti species block the channel, preventing the effective contact between the H_2O_2 solution and active center. The conversion of TS-1-30 is slightly higher than that of the TS-1-120, while the PO yield of the former is much less than the latter. The inverse relationship should be due to the presence of the non-framework Ti species (see Fig. 2). The acidic non-framework Ti species can convert the PO to other by-products and reduce the yield of PO. This result is consistent with that obtained on the classical TS-1 synthesised with TPAOH.[13] In a vapor-phase epoxidation of propene, the absorbed PO may open the ring to form branched alkanes, which are subsequently converted into polyalkenes, propanal and so on.[20–23] The side reaction of PO lowers the selectivity of the TS-1 catalyst unquestionably. Therefore, the acidic non-framework Ti species in TS-1-30 sample should be eliminated.

3.3 Acid treatment of TS-1 with the $SiO_2/TiO_2 = 30$

3.3.1 The influence of the sequence of calcination and acid treatment. The non-framework Ti species is harmful for propylene epoxidation according to the above results. The acid treatment procedure was used to eliminate the non-framework Ti species. Fig. 10 shows the UV-Vis spectra of the TS-1 samples treated with hydrochloric acid ($C_{HCL} = 1.0$ mol L^{-1}) in different post-treatment sequences.[24] The UV-Vis spectra show that a considerable amount of non-framework Ti species were observed on both the as-synthesized (curve a) and calcined (curve b) samples. The peak shifts to a high-wavelength side, which means that a part of the amorphous TiO_2 was transformed into the anatase TiO_2. It is clear that only a small amount of the amorphous Ti species and the anatase TiO_2 were removed when the samples were treated by HCl after the calcination (curve d). It seems that once the anatase TiO_2 is formed, it is difficult to eliminate it by HCl washing treatment alone. Therefore, it is important that the amorphous TiO_2 is removed before it is transformed into anatase TiO_2 by the calcination step. As expected, most of the non-framework Ti species are eliminated after acid washing treatment, before the calcination step (Fig. 10c). At the same time, the concentration of the framework Ti species (220 nm) has not been obviously affected. These results indicate that the sequence of post treatment is the key to the efficient elimination of the non-framework TiO_2.

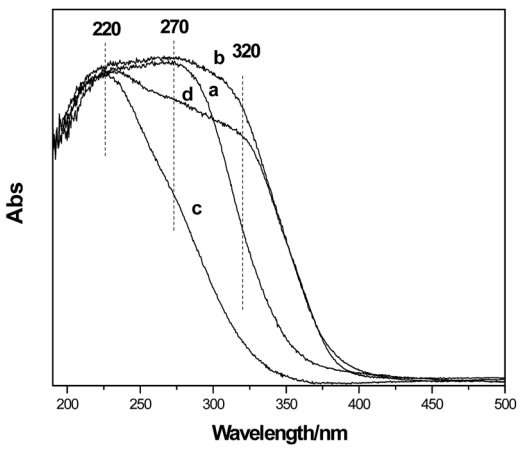

Fig. 10 UV-Vis spectra of the TS-1 samples ($SiO_2/TiO_2 = 30$) modified by the different post-treatments. (a) Dry; (b) dry-calcine; (c) dry-acid treating-calcine; (d) dry-calcine-acid treating-calcine.

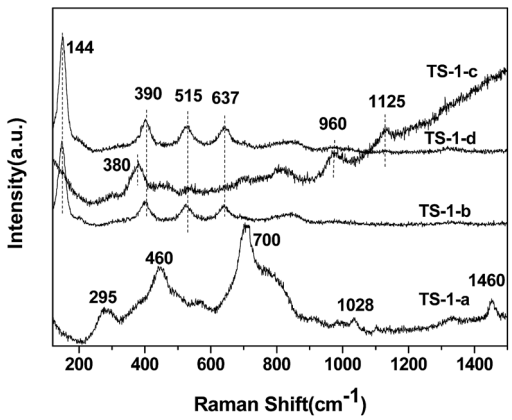

Fig. 11 Raman spectra of the TS-1 samples ($SiO_2/TiO_2 = 30$) modified by different post-treatments (325 nm). (a) Dry; (b) dry-calcine; (c) dry-acid treating-calcine; (d) dry-calcine-acid treating-calcine.

Fig. 11 shows the Raman spectra of the TS-1 samples modified by different post-treatments with the use of 325 nm line. The as-synthesized sample (TS-1-a) shows the intense Raman bands at 295, 460, 700, 1028 and 1460 cm^{-1}. The bands appearing at 295 cm^{-1} and 460 cm^{-1} are the five-membered ring structure and the bending vibration of Si–O, respectively.[25] The band at 700 cm^{-1} is typical for the amorphous Ti species. The latter two are associated with TPAOH. No Raman bands at 144, 390, 515 and 637 cm^{-1} are observed, indicating the absence of anatase TiO_2. After the calcination (b) these peaks appear, indicating the formation of the anatase TiO_2. It is clear that the following acid treatment and calcination (d)

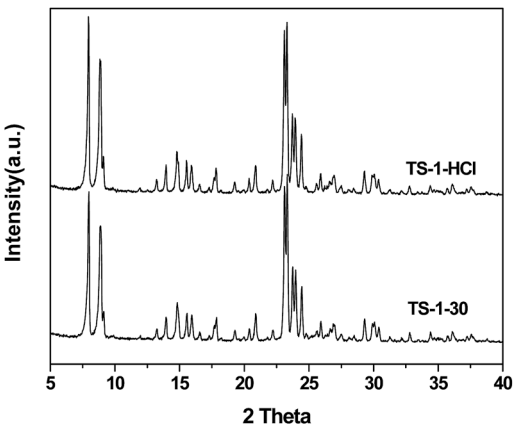

Fig. 12 XRD patterns of TS-1 samples before and after HCl washing.

cannot eliminate the anatase TiO_2. However, if the acid treatment is performed before the calcination step (c), no anatase TiO_2 can be found in the spectrum. The bands at 380, 960 and 1125 cm^{-1}, which are associated with the framework of TS-1, were clearly observed. The results reveal that the anatase TiO_2 cannot be removed once the samples are calcined prior to acid treatment. The above result is in agreement with the UV-Vis spectroscopy result. Therefore, the TS-1 was treated with HCl prior to calcination in the following sections.

Fig. 12 shows the XRD patterns of the TS-1 samples before and after the HCl acid treatment. It is clear that the sample keeps the MFI topology structure perfectly after acid treatment.

3.3.2 The influence of different acid modifiers on acid treatment. To study the effects of different types of acids on the elimination of non-framework TiO_2, HCl, H_2SO_4, HNO_3, H_3PO_4 and H_3BO_3 were used as acid modifiers ($C_{(H^+)}$ = 1.0 mol L^{-1}). The UV-Vis spectra of the TS-1-30 samples before and after acid treatments are shown in Fig. 13. As a reference, the spectrum of the TS-1-30 sample treated with distilled water is also provided. The treatment with only distilled water shows a slight elimination effect on the non-framework TiO_2 (see the bands at 270 nm and 320 nm). It is clear that the effect of the acid treatment can be divided into two parts. The H_3PO_4 and H_3BO_3-related samples, which belong to relatively weak acids, show the elimination effect similar to that of the distilled water. In contrast, the strong acids such as HCl, H_2SO_4 and HNO_3 show a dramatic effect on eliminating the non-framework Ti species. This indicates that the strong acid is much more effective than the weak acid on the elimination process. This result is confirmed by Raman (see part B, Fig. S1 in the ESI†).

3.3.3 The influence of the acid concentration. The TS-1 samples were washed in HCl solution with different concentrations (0–2.0 mol L^{-1}) to investigate the effect of the acid concentration. As shown in Fig. 14, the intensities of the bands at 270 nm and 310 nm decrease with increasing HCl concentrations (0–0.5 mol L^{-1}). When the HCl concentration reaches 0.5 mol L^{-1}, most of the non-framework Ti species are eliminated, but the framework Ti species is not significantly affected. When the HCl concentration further increases to 2.0 mol L^{-1}, the band at 210 nm, associated with the framework Ti species, shows a slight reduction. This result is also confirmed by the result achieved using Raman (see part B, Fig. S2 in the ESI†).

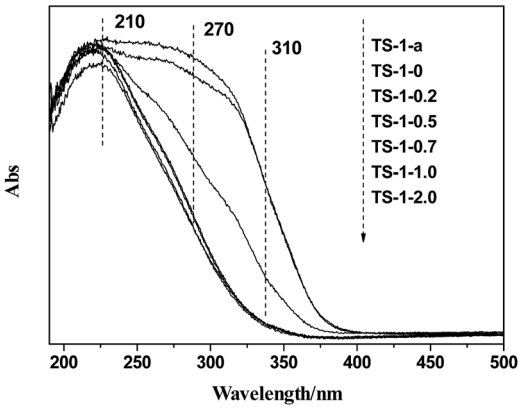

Fig. 14 UV-Vis spectra of the TS-1 samples modified by HCl solution with different concentrations.

In conclusion, almost all the non-framework Ti species can be eliminated, while the framework Ti species is barely influenced by choosing the appropriate HCl concentration (0.5–1.0 mol L^{-1}).

3.3.4 Textural properties of TS-1-30 samples before and after acid washing. Depending on the above results, the TS-1-0.7 sample was chosen for the GC-Raman experiment. Fig. 15 shows the nitrogen physisorption isotherms of TS-1 samples before and after HCl washing. All TS-1 samples exhibit the same type of the nitrogen physisorption isotherm. However, the BET surface areas, microporous surface areas and pore volumes of the treated samples increase in comparison to the as-synthesized sample (see Table 2). This change demonstrates that the elimination of non-framework Ti species, by the acid treatment, may improve the diffusion ability of the zeolite.

3.3.5 The results of *in situ* GC-Raman technique. The *in situ* GC-Raman experiment was performed on the TS-1-30 before

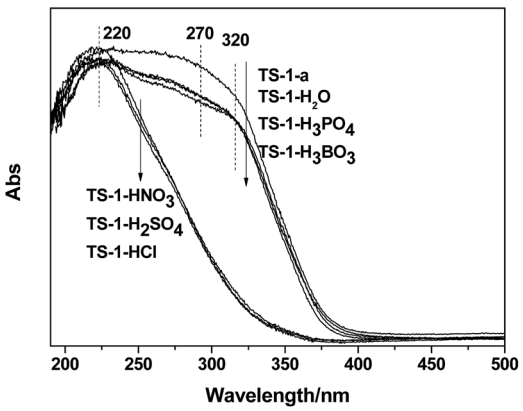

Fig. 13 UV-Vis spectra of the TS-1-30 samples modified by different modifiers.

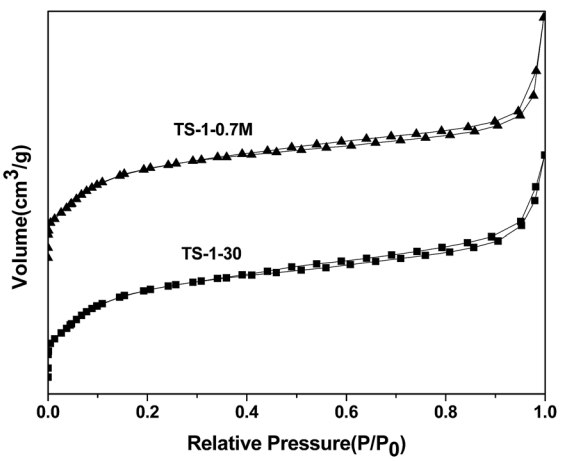

Fig. 15 N_2 adsorption isotherms of TS-1 samples modified by 0.7 M HCl.

Table 2 Textural properties of TS-1 samples modified by acid

Samples	S_{BET} (m^2 g^{-1})	S_{micro} (m^2 g^{-1})	S_{ext} (m^2 g^{-1})	V_{total} (cm^3 g^{-1})	V_{micro} (cm^3 g^{-1})	V_{meso} (cm^3 g^{-1})
TS-1-30	389.9	355.1	34.8	0.2382	0.1501	0.0881
TS-1-0.7	401.9	372.5	29.4	0.2518	0.1575	0.0943

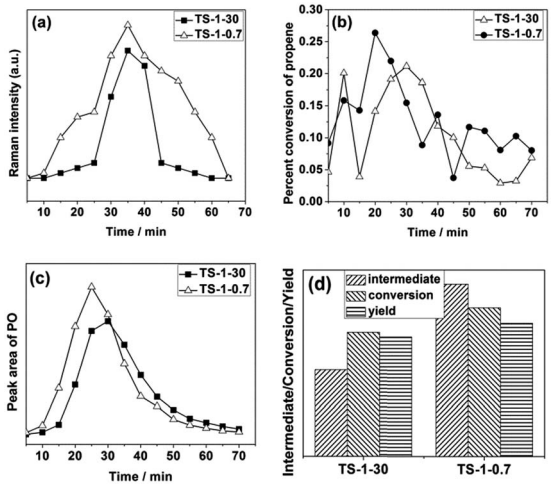

Fig. 16 (a) UV-Raman intensity of the 837 cm^{-1} band at different times during the epoxidation reaction. (b) The conversion of propene in the TS-1/H_2O_2–H_2O/CH_3OH system at different times. (c) The peak area of PO in the GC spectra at different times. (d) The total column of the intermediate, conversion and yield with different SiO_2/TiO_2 ratios.

and after acid washing. The Raman spectra of the TS-1-30 and TS-1-0.7 samples are shown in the part B, Fig. S3 in the ESI.†

As shown in Fig. 16d, the amount of the active intermediate Ti–OOH(η^2), conversion and PO yield are increased after the acid washing treatment step. This indicates that the elimination of the non-framework TiO_2 species favors the formation of the active intermediate Ti–OOH(η^2) and PO. This is most likely due to two possible reasons: (1) the acid treatment may improve the diffusion property of the zeolite by removing the non-framework TiO_2, thus facilitating the contact between the framework Ti species and H_2O_2. (2) The opening reaction of the PO is inhibited by elimination of the acidic non-framework TiO_2. Therefore, the *in situ* GC-Raman results indicate that the conversion and PO yield can be improved by the elimination of the non-framework TiO_2 by a proper acid treatment procedure.

4. Conclusions

The acid treatment on the low-cost TS-1 was systematically investigated using various techniques. The results demonstrate that the framework Ti species is the active center for low-cost TS-1 zeolite. The existence of the non-framework Ti species influences the amount of Ti–OOH(η^2) and reduces the yield of PO. The acid treatment step was used to eliminate the non-framework TiO_2. It was found that the acid treatment of the as-synthesized TS-1 before the calcination is key to efficiently eliminate the non-framework TiO_2. During the calcination process, the amorphous TiO_2 can be transformed into anatase TiO_2, which is difficult to be removed following acid treatment. The strong acids are more efficient for elimination of the non-framework TiO_2 than the relatively weak acids. After treatment with 0.5–1.0 mol L^{-1} HCl solution, most of the non-framework Ti species were eliminated, while the framework Ti species was maintained. As a result, the amount of active intermediate Ti–OOH (η^2), the conversion of propylene and the yield of PO can be improved through acid treatment with appropriate concentration.

Acknowledgements

This study was financially supported by the National Science Foundation of China(NSFC, Grant 21473016).

References

1 M. Taramasso, G. Perego and B. Notari. Preparation of porous crystalline synthetic material comprised of silicon and titanium oxides, *US Pat.*, 4410501, 1983.
2 A. Thangaraj, M. J. Eapen, S. Sivasanker, *et al.*, Studies on the synthesis of titanium silicalite, TS-1, *Zeolites*, 1992, **12**(8), 943–950.
3 G. Li, X. Guo, X. Wang, *et al.*, Synthesis of titanium silicalites in different template systems and their catalytic performance, *Appl. Catal., A*, 1999, **185**(1), 11–18.
4 J. Fang, J. Li, B. Zhang, *et al.*, Support Effect on the Size and Catalytic Activity of Thiolated Au_{25} Nanoclusters as Precatalyst, *Nanoscale*, 2015, **7**(14), 6325–6233.
5 B. Zhang, J. Fang, J. G. Li, *et al.*, Soft, Oxidative Stripping of Alkyl Thiolate Ligands from Hydroxyapatite-Supported Gold Nanoclusters for Oxidation Reactions, *Chem.–Asian J.*, 2016, **11**(4), 532–539.
6 X. J. Deng, Y. N. Wang, L. Shen, *et al.*, Low-Cost Synthesis of Titanium Silicalite-1 (TS-1) with Highly Catalytic Oxidation Performance through a Controlled Hydrolysis Process, *Ind. Eng. Chem. Res.*, 2013, **52**(3), 1190–1196.
7 U. Müller and W. Steck, Ammonium-Based Alkaline-Free Synthesis of MFI-Type Boron- and Titanium Zeolites, *Stud. Surf. Sci. Catal.*, 1994, **84**, 203–210.
8 G. Li, X. Guo, X. Wang, *et al.*, Synthesis of titanium silicalites in different template systems and their catalytic performance, *Appl. Catal., A*, 1999, **185**(1), 11–18.
9 S. T. Tsai, P. Y. Chao, T. C. Tsai, *et al.*, Effects of pore structure of post-treated TS-1 on phenol hydroxylation, *Catal. Today*, 2009, **148**(1–2), 174–178.
10 Y. Wang, M. Lin and A. Tuel, Hollow TS-1 crystals formed *via* a dissolution–recrystallization process, *Microporous Mesoporous Mater.*, 2007, **102**(1–3), 80–85.

11 Y. Wang and A. Tuel, Nanoporous zeolite single crystals: ZSM-5 nanoboxes with uniform intracrystalline hollow structures, *Microporous Mesoporous Mater.*, 2008, **113**(1), 286–295.

12 V. Bolis, S. Bordiga, C. Lamberti, *et al.*, A calorimetric, IR, XANES and EXAFS study of the adsorption of NH3 on Ti-silicalite as a function of the sample pre-treatment, *Microporous Mesoporous Mater.*, 1999, **30**(1), 67–76.

13 G. Xiong, Y. Cao, Z. Guo, *et al.*, The roles of different titanium species in TS-1 zeolite in propylene epoxidation studied by *in situ* UV Raman spectroscopy, *Phys. Chem. Chem. Phys.*, 2016, **18**, 190–196.

14 G. Qiang, S. Keju, F. Zhaochi, *et al.*, A thorough investigation of the active titanium species in TS-1 zeolite by *in situ* UV resonance raman spectroscopy, *Chemistry*, 2012, **18**(43), 13854–13860.

15 C. Li, G. Xiong, Q. Xin, *et al.*, UV-Resonanz-Raman-spektroskopischeIdentifizierung von TitanatomenimGerüst des Zeoliths TS-1, *Angew. Chem.*, 1999, **111**(15), 2358–2360.

16 L. Wang, G. Xiong, J. Su, *et al.*, *In Situ* UV Raman Spectroscopic Study on the Reaction Intermediates for Propylene Epoxidation on TS-1, *J. Phys. Chem. C*, 2012, **116**(116), 9122–9131.

17 G. Ricchiardi, A. Damin, S. Bordiga, *et al.*, Vibrational Structure of Titanium Silicate Catalysts. A Spectroscopic and Theoretical Study, *J. Am. Chem. Soc.*, 2001, **123**(46), 11409–11419.

18 M. A. Camblor, A. Corma and J. Pérez-Pariente, Synthesis of titanoaluminosilicatesisomorphous to zeolite Beta, active as oxidation catalysts, *Zeolites*, 1993, **13**(2), 82–87.

19 J. Su, G. Xiong, J. Zhou, *et al.*, Amorphous Ti species in titanium silicalite-1: Structural features, chemical properties, and inactivation with sulfosalt, *J. Catal.*, 2012, **288**(4), 1–7.

20 S. Bordiga, A. Damin, F. Bonino, *et al.*, Resonance Raman effects in TS-1: the structure of Ti(IV) species and reactivity towards H_2O, NH_3 and H_2O_2: an *in situ* study, *Phys. Chem. Chem. Phys.*, 2003, **5**(20), 4390–4393.

21 B. S. Uphade, T. Akita, T. Nakamura, *et al.*, Vapor-Phase Epoxidation of Propene Using H_2 and O_2 over Au/Ti-MCM-48, *J. Catal.*, 2002, **209**, 331–340.

22 X. Feng, N. Sheng, Y. B. Liu, *et al.*, Simultaneously Enhanced Stability and Selectivity for Propene Epoxidation with H_2 and O_2 on Au Catalysts Supported on Nano-Crystalline Mesoporous TS-1, *ACS Catal.*, 2017, **7**, 2668–2675.

23 X. Feng, Y. B. Liu, Y. C. Li, *et al.*, Au/TS-1 Catalyst for Propene Epoxidation with H_2/O_2: A Novel Strategy to Enhance Stability by Tuning Charging Sequence, *AIChE J.*, 2016, **62**(11), 3963–3972.

24 L. Kong, G. Li and X. Wang, Kinetics and Mechanism of Liquid-Phase Oxidation of Thiophene over TS-1 Using H_2O_2 Under Mild Conditions, *Catal. Lett.*, 2004, **92**(3), 163–167.

25 E. Astorino, J. B. Peri, R. J. Villey, *et al.*, Spectroscopic characterization of silicalite-1 and titanium silicalite-1, *J. Catal.*, 1995, **157**(2), 482–500.

